Astrophysical Sources as Dark Matter Detectors

Jacob Pilawa,
(Cosmin Ilie)

Department of Physics and Astronomy, Colgate University,
Physics 492: Honors Thesis.

E-mail: jpilawa@colgate.edu

Abstract. After scattering off of nucleons inside of stars, dark matter particles can lose enough kinetic energy to be captured in the interior. Subsequently, dark matter self-annihilation provides an additional heating source for these objects, opening a new avenue to constrain dark matter properties. Extending previous work on the single-scatter and multi-scatter formalisms of dark matter capture, we show that old neutron stars in the Milky Way's center and Population III stars can constrain the dark-matter cross section below the limit of direct detection experiments in the mass range of $m_\chi \approx 10^1\,\mathrm{GeV} - 10^8\,\mathrm{GeV}$. This gives hope to extending our search below the neutrino floor and beyond the Standard Model.

Contents

1 Introduction

The precise nature of dark matter is an unsolved mystery of modern astrophysics. Two methods of detection experiments have emerged – a first camp of ground-based direct detection experiments [1, 2] that detect interactions of dark matter scattering off of nuclei in deep underground detectors; and a second camp of astrophysical sources of dark matter annihilation [3, 4]. Both of these approaches have constrained dark matter properties, but are limited in scale. Direct-detection experiments are reaching physical limitations set by the sensitivity of the experiments, and astrophysical sources typically cannot reach as low of bounds as direct-detection.

More recent attempts at astrophysical constraints of dark matter properties have explored the evolution of stars. If dark matter is captured and annihilates, a detectable flux is released from these sources. There are two main capture mechanisms for this dark matter to reach the center of the star: (a) adiabatic contraction and (b) capture. Adibatic contraction is a phenomenon that results from baryonic infall to the star. As the center of the gravitational well continues to accrete mass, the potential grows larger and larger until the inner, orbiting dark matter falls inward [5]. Capture, on the other hand, involves dark matter transiting the object. On its journey through the star, the dark matter particle will scatter off of nucleons until the velocity is lower than the escape velocity, providing a non-zero accretion rate of dark matter into the star [6]. This second mechanim is the focus of this paper.

Generally, there are three scenarios for capture, characterized by the average number of scatters until capture N. When $N \sim 1$, we are in the "single-scatter" regime studied by Freese [6] and Gould [7] for stars and for the Earth, respectively. The number of scatters is a proxy for the mass of the dark matter being captured, and for scatters around 1, we have approximately the WIMP mass (10^2 GeV). When $N \gg 1000$, we can refer to the approximation of Albuquerque's SIMPZILLA [8] which is extremely massive but strongly interacting, causing a huge number of scattering events for capture. More recent studies [9, 10] have introduced a multiscatter formalism to calculate multiscatter

capture rates and the subsequent luminosity from the additional heating source of dark matter annihilation, providing a new by means which we can detect and constrain dark matter across all mass and cross section regimes.

In this paper, we extend the multiscatter formalism to include both full expressions and semi-analytic capture rates. We then apply this formalism in the context of white dwarfs, neutron stars, and Population III stars to examine the potential of this method to constrain dark matter properties more sensitively than direct-detection experiments. The paper will be organized as follows. Section 2 will introduce the multiscatter capture formalism and extend it to semi-analytic expressions for the capture rate; Section 3 will show this formalism in context, applying these methods to white dwarfs; Section 4 will analyze neutron stars in the Milky Way's galactic center in the context of dark matter self-annihilation; Section 5 will show that future space-based observatories can use Population III stars to supplement the constraints from neutron stars; and, Section 6 will summarize the work, providing direction for future research into this area of study.

2 Formalism of Multiscatter Capture

In this section, we derive the multi-scatter capture formalism and several useful semi-analytic approximations for analyzing the interactions of dark matter inside stars. We consider a dark matter particle traversing through a star, losing energy with each recoil off a nucleon. The average number of scatters the dark matter particle will undergo is thus approximated by

$$N \approx 2 n_T \sigma_n R_\star \tag{2.1}$$

where n_T is the number density of collision targets, σ_n is the scattering cross section between dark matter and nucleons, and $R_\star$ is the radius of the star the particle is transiting. Two situations thus arise. In the case of dark matter masses $m_\chi \sim 100\,\mathrm{GeV}$, the average number of collisions is always less than unity in view of the small scattering cross sections for lightweight dark matter ($\sigma_{SI} \lesssim 10^{-46}\,\mathrm{cm}^2$) [11]. However, heavier dark matter loses less energy per collision than its lighter counterparts, requiring a larger number of collisions until successful capture. Because the mass range we are working with contains both single-scatter and multi-scatter regimes, we need to this multi-scatter approach.

As massive dark matter enters the interior of the star, the larger cross sections mean that the mean free path of these particles is very short. Dependent on the scattering angle, the fractional energy loss per collision can be expressed as

$$0 \leq \frac{\Delta E_i}{E_i} \leq \beta_+. \tag{2.2}$$

In the above equation, we introduce the parameter $\beta_+ \equiv 4 m_\chi m_n / (m_\chi + m_n)^2$. Assuming equal probability of all fractional energy changes, we find an average fractional kinetic energy loss of $\beta_+/2$. We then must consider the factors that will influence the capture rate itself. The two primary factors controlling this phenomenon are the flux

F of dark matter through the star and the probability Ω that the dark matter will undergo sufficient numbers of collisions to be captured. This gives rise to a differential capture rate of

$$\frac{dC}{dVd^3u} = dF\left(n_\chi, u, v_\star, v_{esc}^{halo}\right)\Omega\left(n_T, w, \sigma_n, m_n, m_\chi\right) \tag{2.3}$$

where u is the velocity of dark matter far away from the gravitational field of the star, $v_\star$ is the relative velocity of the star with respect to the halo, v_{esc}^{halo} is the escape velocity of the dark matter halo, n_T is the number density of scattering targets as a function of radius of the halo, $w^2 = u^2 + v_{esc}^2$ is the velocity of dark matter inside of the star with $v_{esc}^2 = 2GM_\star/r$. Since Pop. III stars form at the centers of their halos, we can assume that $v_\star \to 0$. We also make the assumption that the halo has a very large escape speed ($v_{esc}^{halo} \to \infty$), a uniform density inside the star, and a fixed escape velocity. Given these assumptions, we can express the total capture rate as a function of dark matter mass as:

$$C_{tot}(m_\chi) = \sum_{N=1}^{\infty} C_N \tag{2.4}$$

where C_N is the capture rate after exactly N scatters. We can construct C_N considering Equation 2.3. We can break Ω into two parts. The first component is the probability of *exactly* N scatters given the average number of scatters expressed above (note: we can think of the average number of scatters as the object depth τ of the star). If we consider all potential scattering angles α, this probability is given by the $P \sim$ Poisson(τ, N) distribution [12]:

$$\begin{aligned} p_N(\tau) &= 2\int_0^1 d\alpha \frac{\alpha e^{-\alpha\tau}(\alpha\tau)^N}{N!} \\ &= \frac{2}{\tau^2}\left(N + 1 - \frac{\Gamma(N+2,\tau)}{N!}\right) \end{aligned} \tag{2.5}$$

The second portion (which we will call $g_N(w)$) of Ω is the probability that the dark matter particle's velocity drops below the escape velocity of the star after exactly N collisions, ensuring full capture. The initial kinetic energy of the dark matter can be expressed as:

$$E_0 = \frac{1}{2}m_\chi w^2. \tag{2.6}$$

Assuming elastic collisions between the dark matter and nucleons, the energy lost after each collision is $\Delta E = z\beta_+ E_0$ where $z \in [0,1]$ is the scattering angle and where β_+ is defined as above. This simplifies the energy after the i'th collision to $E_i = (1 - z\beta_+)E_{i-1}$. This, in turn, makes the velocity after the i'th collision $v_i = (1 - z\beta_+)^{1/2}v_{i-1}$. We can make a simplifying assumption that $m_\chi \gg m_n$, making $\beta_+ \approx 4\frac{m_n}{m_\chi}$. We can generalize these expressions to the calculate the energy and velocity

after exactly N scatters[12]:

$$E_N = \prod_{i=1}^{N} (1 - z_i\beta_+)\, E_0. \tag{2.7}$$

$$v_N = \prod_{i=1}^{N} (1 - z_i\beta_+)^{1/2}\, w. \tag{2.8}$$

We can now define a function $\Theta(x)$ such that $\Theta(x) = 1$ if $x > 0$. We can use this, as well as the initial velocity, to find the probability that the dark matter particle's velocity dips below the escape velocity after N scatters.

$$g_N(w) = \int_0^1 dz_1 \cdots \int_0^1 dz_N \Theta\left(v_{esc} \prod_{i=1}^{N} (1 - z_i\beta_+)^{-1/2} - w\right) \tag{2.9}$$

This integration over the infinitesimal scattering angles dz_i is a summation for all possible trajectories. The expression in parentheses essentially checks the condition that a dark matter particle with initial velocity w can, in fact, be captured after exactly N collisions. We can simplify the entire integral by averaging over all scattering angles z_i. The average value of this is $\langle z_i \rangle = 1/2$. Therefore, $g_N(w)$ simplifies to:

$$g_N(w) = \Theta\left(v_{esc} \prod_{i=1}^{N} (1 - z_i\beta_+)^{-1/2} - w\right). \tag{2.10}$$

The total capture rate is thus the product of the proability of capture and the dark matter flux. This capture rate C_N can be expressed as:

$$C_N = \pi R^2 p_N(\tau) \int_0^\infty f(u) \frac{dw}{u^2} w^3 g_N(w) \tag{2.11}$$

Integrating this expression over velocity space, we obtain:

$$C_N = \pi R^2 p_N(\tau) \frac{\sqrt{2} n_\chi}{\sqrt{3\pi}\bar{v}} \left(\left(2\bar{v}^2 + 3v_{esc}^2\right) - \left(2\bar{v}^2 + 3v_N^2\right) \exp\left(-\frac{3\left(v_N^2 - v_{esc}^2\right)}{2\bar{v}^2}\right)\right) \tag{2.12}$$

with $v_N = v_{esc}\,(1 - \beta_+/2)^{-N/2}$. In the limit that $v_{esc} \gg \bar{v}$ and $m_\chi \gg_n$, this expression becomes:

$$C_N = \sqrt{24\pi} p_N(\tau) n_\chi G M_\star \frac{1}{\bar{v}} \left(1 - \left(1 + \frac{2A_N^2\bar{v}^2}{3v_{esc}^2}\right) e^{-A_N^2}\right) \tag{2.13}$$

where

$$A_N^2 = \frac{3v_{esc}^2 N m_n}{\bar{v}^2 m_\chi} \tag{2.14}$$

If we consider Equation 2.12 for large N, we see that the capture rate after exactly N scatters goes to $C_N \approx 0$ when the number of scatters is larger than τ. It

is therefore convenient to derive expressions for the mass-capture rate $C_{tot}m_\chi$ after k scatters ($C^{\mathbf{k}}m_\chi$) in the large dark matter mass and small dark matter mass cases. These are non-trivial calculations but can be derived using from the definitions of $p_N(\tau)$. It is worth noting that, for a given star, all of the following expressions are simply a function of m_χ. We find:

$$\mathrm{C}^{\mathbf{k}}m_\chi = \begin{cases} \pi R^2 \frac{\sqrt{2}n_\chi}{\sqrt{3\pi}\bar{v}} \left(2\bar{v}^2 + 3v_{esc}^2\right) \frac{k(k+3)}{(n_T\sigma_{nX}2R)^2} m_\chi & ; \frac{3\left(v_N^2 - v_{esc}^2\right)}{2\bar{v}^2} \gg 1, k < \tau \\ \pi R^2 \frac{\sqrt{3}n_\chi}{\sqrt{2\pi}\bar{v}^3} 3v_{esc}^4 z_i 4m_N \frac{2}{\tau^2} \left[\frac{k(k+1)(k+2)}{3} + z_i \frac{4m_N}{m_\chi} \frac{k(k+1)(k+2)(3k+1)}{12}\right] & ; \frac{3\left(v_N^2 - v_{esc}^2\right)}{2\bar{v}^2} \ll 1, k < \tau \\ \pi R^2 \frac{\sqrt{2}n_\chi}{\sqrt{3\pi}\bar{v}} \left(2\bar{v}^2 + 3v_{esc}^2\right) m_\chi & ; \frac{3\left(v_N^2 - v_{esc}^2\right)}{2\bar{v}^2} \gg 1, k > \tau \\ \pi R^2 \frac{\sqrt{3}n_\chi}{\sqrt{2\pi}\bar{v}^3} 3v_{esc}^4 z_i 4m_N \left[\frac{2\tau}{3} + z_i \frac{4m_N}{m_X} \frac{\tau^2}{2}\right] & ; \frac{3\left(v_N^2 - v_{esc}^2\right)}{2\bar{v}^2} \ll 1, k > \tau \end{cases} \tag{2.15}$$

Armed with the above analytic expressions as a function of scatter number k, as well as the more general total capture rate expression (2.12), we can look at the implications of dark matter capture in white dwarf stars before moving to exotic environments in which we can constrain dark matter properties.

3 Mutliscatter Capture in Context

White dwarfs are remnants of main-sequence stars which are supported by electron-degeneracy pressure. These, and other compact objects, have been studied in the single scatter regime [13–15], but in the multiscatter regime there is little work. They are primarily composed of carbon and oxygen $m = m_n = \mathcal{O}(10\,\mathrm{GeV})$, so we are still in the regime where the multiscatter formalism holds. The advantage of the multiscatter formalism is that we can probe larger dark matter masses. To explore the properties of dark matter annihilation in these environments, a few computational intracices must be adjusted [10]. First, the spin-dependent dark matter interactions at high energies will be suppressed by a form factor. We therefore modify the cross section as:

$$\sigma \to \sigma_{n\chi} \frac{M_N^4}{m_n^4} F^2\left(\langle E_R \rangle\right) \tag{3.1}$$

where m_n is the mass of nucleons in a hydrogen-dominant star and M_N is the mass of nucleons in white dwarfs. $F^2\left(\langle E_R \rangle\right)$ is the Helm form factor evaluated at the average recoil energy which is ~ 0.5 [10]. We also must adjust the average scatter angle $\langle z_i \rangle$ since these interactions are happening at much higher energies. To account for this, $\langle z_i \rangle \to \langle E_R \rangle / E_R^{max}$.

We assume for our calculations that a constant density white dwarf of mass $1M_\odot$ and radius $R = 10^4\,\mathrm{km}$ captures dark matter with nucleon-cross sections of $\sigma_{n\chi} = 10^{-38}\,\mathrm{cm}^2$ and $10^{-36}\,\mathrm{cm}^2$. The results of these mass-capture calculations are presented in Figure 1 where we have included our expressions for $C_{tot}m_\chi$ and $C^{\mathbf{k}}m_\chi$.

As we increase the interaction cross section (left-side of Figure 1 to right-side of Figure 1), we notice a few things. First, the single scatter mass capture rate decreases dramatically. This is a consequence of the fact that, for larger cross-section, more

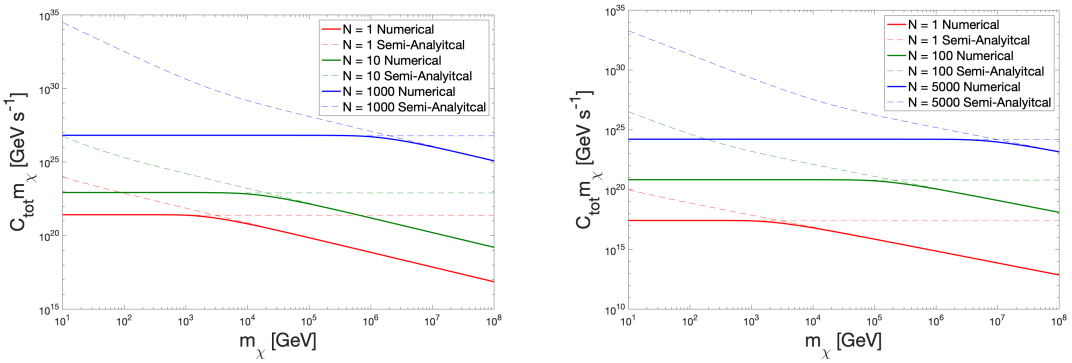

Figure 1: Mass capture rate as a function of m_χ for a white dwarf with the mass and radius specified below. The capture rate was calculated for scatter numbers $N = 1, 10, 1000$ (left) and $N = 1, 10, 5000$ (right). Both the full numerical $C_{tot}m_\chi$ and $C^{\mathbf{k}}m_\chi$ are plotted and are in agreement in both high and low mass regimes. The left panel uses an interaction cross section of $\sigma_{n\chi} = 10^{-38}\,\mathrm{cm}^2$ and the right panel uses $\sigma_{n\chi} = 10^{-36}\,\mathrm{cm}^2$.

scattering events are needed so the single scatter case under predicts the total capture rate. There is also an interesting feature in the point in which the curves turn over from $C_{tot} = \text{const.}$ to $C_{tot} \propto m_\chi^{-1}$. This comes from the fact that the energy loss for each collisions scales as m_χ^{-1}, so lighter dark matter require fewer scatters to be captured. As you increase the dark matter mass, you need more scattering events for complete capture and thus the capture rate decreases with mass.

It should be noted that the cross sections that were used are well above the detection limit of ground-based dark matter detection facilities. These cross sections were used to draw a comparison between the single scatter and multiscatter regimes.

We can see the utility in astrophysical sources by next considering neutron stars. The same process for white dwarf capture holds, but there first need to be corrections to the kinetic energy of particles in the rest from of a distant observer and C_N to account for general relativistic effects [10]. First, the gravitational potential around a white dwarf is enhanced from a Newtonian potential which will increased the capture rate by a factor of $\left(1 - \frac{2GM}{Rc^2}\right)^{-1}$. This modifies the capture rate after N scatters to:

$$C_N \to \frac{C_N}{1 - \frac{2GM}{Rc^2}} \tag{3.2}$$

We can then correct for the gravitational blue-shift by modifying v_{esc}. The initial kinetic energy will be enhanced by a factor $\chi = \left[1 - \left(1 - \frac{2GM}{Rc^2}\right)^{1/2}\right]$:

$$v_{esc} \to \sqrt{2\chi} \tag{3.3}$$

Making these substitutions, we can examine the mass capture rate of dark matter inside neutron stars just as we did for white dwarfs. We consider the case of a $1.5M_\odot$ neutron star with radius $R = 10\,\mathrm{km}$ and an ambient dark matter density of $\rho_\chi = 0.3\,\mathrm{GeV/\,cm}^3$. The results of this calculation are presented in Figure 2.

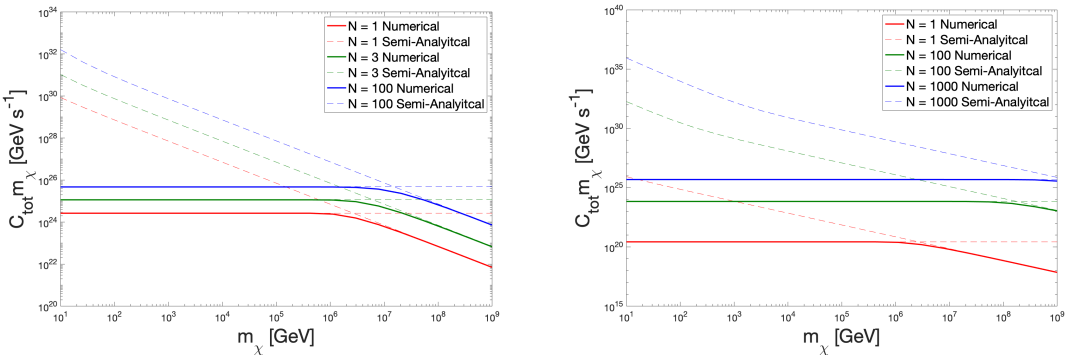

Figure 2: Mass capture rate as a function of m_χ for a neutron star. The capture rate was calculated for scatter numbers $N = 1, 3, 100$ (left) and $N = 1, 100, 1000$ (right). Both the full numerical $C_{tot} m_\chi$ and $C^{\mathbf{k}} m_\chi$ are plotted and are in agreement in both high and low mass regimes. The left panel uses an interaction cross section of $\sigma_{n\chi} = 10^{-44}\,\mathrm{cm}^2$ and the right panel uses $\sigma_{n\chi} = 10^{-42}\,\mathrm{cm}^2$.

Qualitatively, these figures are similar to Figure 1 for the same reasons as described above. However, we need to decrease the interaction cross section significantly for mass capture rate to be of similar order to the white dwarf case. This is the first hint of astrophysical sources being used to constrain dark matter properties at limits smaller than ground-based direction detection experiments like XENON1T [1] and PandaX-II [2]. Additionally, there is promising preliminary research that uses Population III stars to constrain dark matter properties similar to neutron stars [9]. The two methods, in conjunction, can push the exclusion limits for interaction cross sections below the sensitivity of the aforementioned ground-based experiements with future space-based facilties like JWST.

4 Constraints from Neutron Stars

Considering Figure 2, we can start to see the feasibility of constraining dark matter properties with astrophysical sources. The annihilation of dark matter inside of neutron stars can affect their temperature in regions of sufficiently high dark matter density such as the Milky Way galactic bulge. While there have been no confirmed neutron stars found in this region, the next generation of radio telescopes will be able to probe deeper into the dust-secluded region, opening up the possibility of detection.

As dark matter thermalizes inside of neutron stars, it settles into the inner regions and can annihilate. This continues until equilibrium is reach, at which point the oldest neutron stars ($T_{NS} \ll 3 \times 10^4 K$) receive a "boost" in temperature due to the dark matter annihilation [10]. We can use this fact to define the effective temperature of the neutron star due to the mass-capture (which, in turn, sets an "effective luminosity"):

$$m_x C_N = L_{DM} = 4\pi\sigma_0 R^2 T_{NS}^4 \left(1 - \frac{2GM}{Rc^2}\right)^2 \tag{4.1}$$

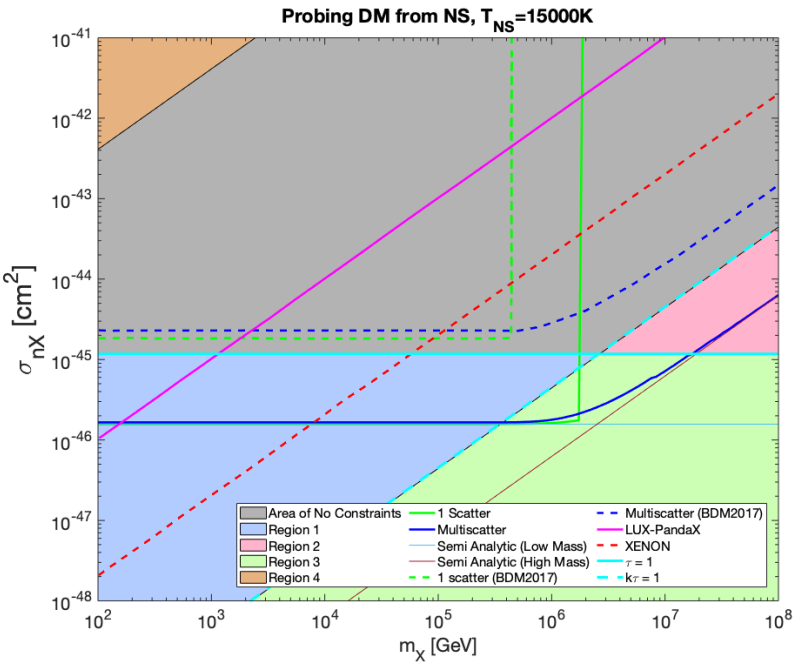

Figure 3: Upper bounds on σ_χ derived from neutron stars from full numerical calculations and semi-analytic calculations in the low and high mass regimes. We assumed an ambient dark matter density of $10^3\,\mathrm{GeV}/cm^3$, a $1.5M_\odot$ neutron star with radius $R = 10\,\mathrm{km}$ and a neutron star temperature of $T = 15,000\,\mathrm{K}$ to ensure capture-annihilation equilibrium is reached. The colors are explained in the paragraphs below, but they correspond to different cases of the formalism and where various approximations hold.

where σ_0 is the Stefan-Boltzmann constant, and where we have corrected for general relativistic effects in the environment of the neutron star. We can make this expression useful by summing the left side over all N and grouping constants on the right that are a function of stellar parameters only and dark matter parameters on the left. Then, for a given set of stellar parameters, we can find σ_χ as a function of m_χ, setting constraints on dark matter through observation. Doing this calculation gives an expression:

$$C_{tot} m_\chi = 1.96 \times 10^{-3}\,\mathrm{GeV\,s^{-1}} \left(\frac{T_{NS}}{T_\odot}\right)^4 \tag{4.2}$$

where C_{tot} itself is a function of σ_χ. Solving 4.1 for $\sigma_\chi(m_\chi)$ gives two different behaviors for bounds on the cross section seen in Figure 3. Current direct detection bounds and bounds derived in [10] are included for ease of comparsion. Additionally, we include the bounds derived from our semi-analytic formalism $C^{\mathbf{k}} m_\chi$ as a consistency check.

First, we notice that we recover the single-scatter formalism from the multiscatter expression derived in this paper in the small mass regime. In this mass range, the bound

σ_χ is independent of dark matter mass. When τ transitions from $\tau \ll 1$ to $\tau \gg 1$ (around $m_\chi \sim 10^7\,\mathrm{GeV}$), the single scatter formalism breaks down and $\sigma_\chi \propto m_\chi$. We have included both the full numerical solution for single and multiscatter, as well as the semi-analytic expressions for the two scattering regimes to show self-consistency and to aid future work.

There are a few other interesting features to mention, denoted by the colored regions in Figure 3. The gray region is an area where there can be no constraints since the sum of probabilities on the left hand side of 4.1 is unity. Any results in this regime are meaningless and cannot be used to constrain dark matter properties. The lower left blue region and upper right red region are the single scatter and multiscatter regimes, respectively, where our formalism holds strongly. The lower left green region is not well understood – the system is "transistioning" in this region from single scatter to multiscatter and can only be understood numerically. We also mark critical boundaries between these two regions in cyan. Hoizontally, we divide the plane into $\tau < 1$ (lower half) and $\tau > 1$ (upper half). Diagonally up and to the right, we divide the plane into $A_N^2 < 1$ (right side) and $A_N^2 < 1$ (left side).

It is an exciting result that the multiscatter regime and formalism allows future space-based astrophysical observatories to probe dark matter properties beyond the detection limit of ground-based direct detection.

5 Constraints from Population III Stars

There is a key difference in the effects of dark matter annihilation in Population III stars compared to the former cases of white dwarfs and neutrons stars. The stellar remnants have negligible nuclear luminosity compared to self-annihilation dark matter luminosity; but in the case of Population III stars, this assumption goes away. We therefore must constrain dark matter properties in Population III stars using the condition that the nuclear and dark matter luminosity sum to the Eddington Luminosity of that object [16].

$$L_{Edd} = \frac{4\pi c G M_\star}{\kappa_\rho} \tag{5.1}$$

In calculating the Eddington luminosity, we introduce κ_ρ as the opacity of the stellar atmosphere. Read left to right, equation 5.1 says that the Eddington luminosity can be calculated for a given stellar mass. However, read from right to left, we place a maximum bound on the mass of stars powered by nuclear fusion and dark matter self-annihilation by imposing that a star shines at the Eddington limit.

Mathematically, we can place two types of bounds which we refer to as the "strong limit" and the "weak limit." The former is taking into account both the nuclear and dark matter luminosity, whereas the latter restricts luminosity to only self-annihilating dark matter. Mathemmatically, these criteria are:

$$\text{Bounds} \rightarrow \begin{cases} L_{edd}(M_{max}) = L_{DM}(M_{max}) + L_{nuc}(M_{max}) & : \text{Strong Limit} \\ L_{edd}(M_{max}) = L_{DM}(M_{max}) & : \text{Weak Limit} \end{cases} \tag{5.2}$$

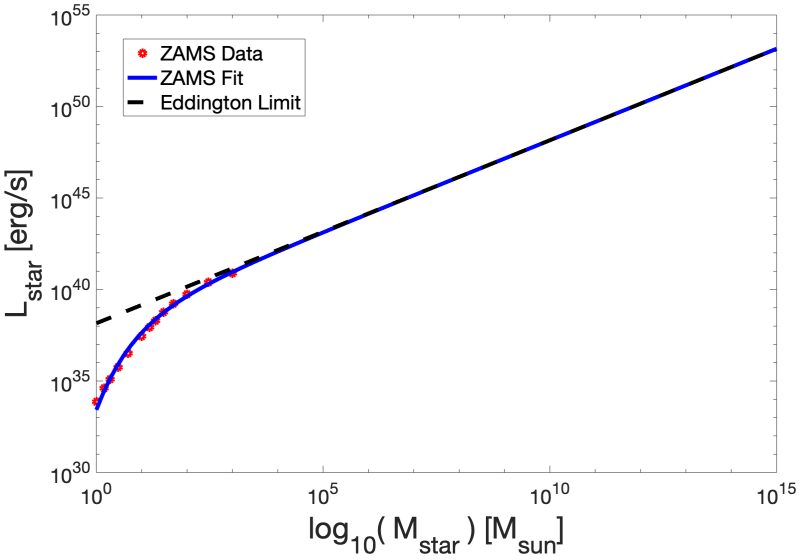

Figure 4: Nuclear luminosity fit for Population III stars.

The reality is that the "true" upper mass bounds will be somewhere in between the two criteria. The weak limit is very weak in that it completely disregards the most prominent heating mechanism (nuclear fusion) for the interiors of the star. The strong limit assumes that the additional heating from dark matter has no effect on hydrogen burning and is therefore missing crucial physics. A detailed analysis of dark matter's effect on hydrogen burning is beyond the scope of this paper.

To calculate these bounds, we begin by constructing a fit for the luminosity of Pop. III stars from simulations found in [17, 18]. The data for these stars are presented in Table 1 and the fit in Figure 4. The fit was constructed assuming main-sequence scaling relations of $L \propto M^5$ for small mass stars, $L \propto M^3$ for medium mass stars, and $L \propto M$ for high mass stars with the additional constraint that $L \to L_{edd}$ as $M \to \infty$. The full function form of the derived equation is

$$L_{nuc} \simeq 10^{\frac{\log\left(3.7142\times10^4 L_\odot \mathrm{s/erg}\right)}{1+\exp(-0.8502x-1.9551)}} \cdot x^{\frac{2.0135}{x^{0.4817}+1}} \,\mathrm{erg/s} \tag{5.3}$$

where $x \equiv \frac{M_\star}{M_\odot}$ and $L_\odot \equiv 3.846 \times 10^{33}\,\mathrm{erg/s}$.

We then need to derive the luminosity from dark matter self-annihilation. The total number of dark matter particles in the star can be modeled by the capture and anihiliation rates

$$\dot{N} = C - 2\Gamma_\mathrm{A} \tag{5.4}$$

where C is the capture rate and Γ_A is the annihilation rate. After equilibrium is reached, the capture and annihilation rates are related by:

$M_\star[M_\odot]$	$R_\star[R_\odot]$	$L_\star[L_\odot]$
1	0.875	1.91×10^0
1.5	0.954	1.05×10^1
2	1.025	3.29×10^1
3	1.119	1.46×10^2
5	1.233	8.46×10^2
10	1.400	7.27×10^3
15	1.515	2.34×10^4
20	1.653	5.11×10^4
30	2.123	1.45×10^5
50	2.864	4.25×10^5
100	4.118	1.40×10^6
300	7.408	6.57×10^6
1000	12.85	2.02×10^7

Table 1: Stellar parameters used in calculations.

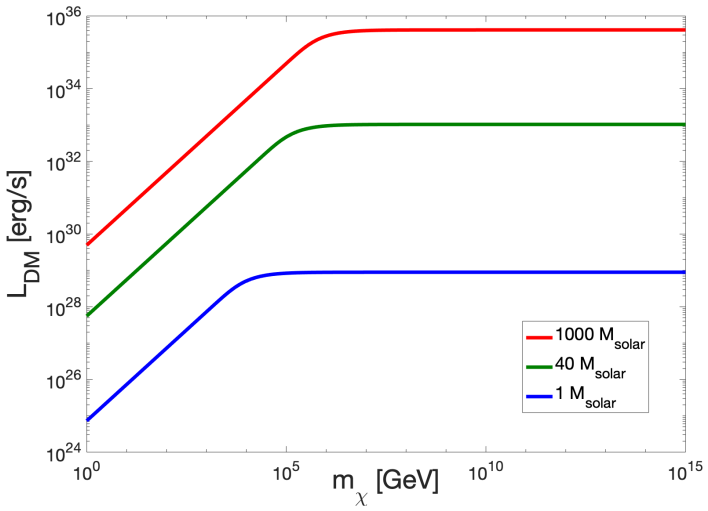

Figure 5: Calculated dark matter luminosity for $M = 1, 40, 1000 M_\odot$.

$$\Gamma_A = \frac{1}{2} C \tag{5.5}$$

This now is a stable heating source for the interior of the star. If we consider a single annihilation, a energy equal to $2m\chi$ is released with some efficiency f. We adopt an efficiency parameter $f = 2/3$[19] in which the $f_{\rm lost} = 1/3$ comes from neutrino outflow from these annihilations. This gives us the ability to calculate the luminosity due to DM-DM interaction.

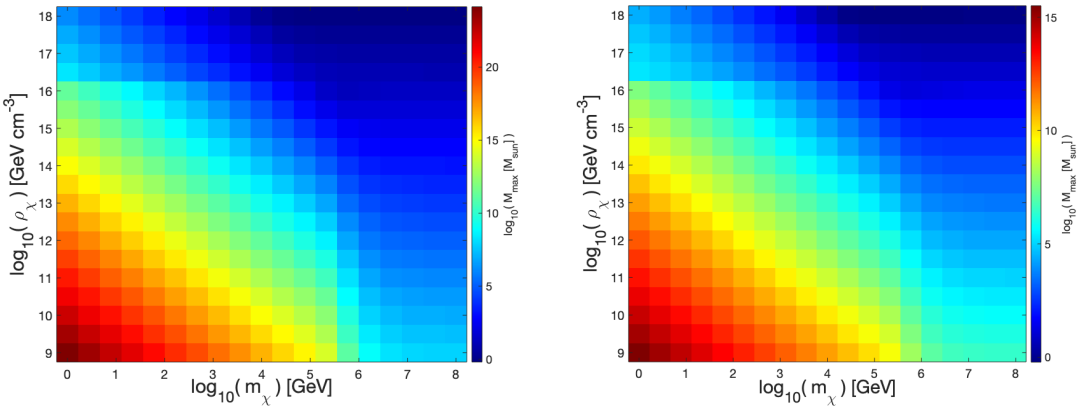

(a) Weak limit. (b) Strong limit.

Figure 6: Maximum stellar mass for a given m_χ and ρ_χ.

$$L_{\rm DM} = \frac{f}{2} C_{\rm tot}\,(2m_\chi) \tag{5.6}$$

We present the calculations for dark matter luminosity in Figure 5 for three stars. We can see that, for lower mass dark matter (and therefore, the single-scatter regime), $L_{\rm DM} \propto m_\chi$; and for higher mass dark matter (well into the multi-scatter regime), $L_{\rm DM}$ is independent of m_χ. There is no straightforward relationship between $L_{\rm DM}$ and m_χ for the intermediate mass regime, but we are still able to computationally analyze the effects on stellar evolution from this additional heat source.

Considering the addition of the dark matter luminosity to the nuclear luminosity, the maximum mass for these stars is thus only a function of the dark matter mass and the corresponding dark matter density. This establishes a two-parameter space to be swept over to calculate these bounds. The results of this parameter sweep are presented in Figure 6.

We note that in the "strong" limit, the luminosity due to nuclear fusion dominates for most of the parameter space. Our calculations place this upper bound at $M_{\rm max} \approx 10^{15} M_\odot$ at small m_χ and small ρ_χ. As we increase the density and dark matter mass to more extreme values, we find the maximum mass approaches $M_{\rm max} \approx 0.1 M_\odot$!

Considering dark matter heating only, we get a much wider range of maximum masses. In the WIMP regime at low central halo densities, dark matter heating allows for absurdly large stellar masses of $M_{\rm max} \gtrsim 10^{24} M_\odot$. However, increasing the density and dark matter mass leads to a smooth, though dramatic, transition from $10^{24} M_\odot$ to $M_{\rm max} \approx 0.1 M_\odot$. We reiterate again that the "real" maximum mass is likely closer to the "strong" limit since nuclear fusion remains the dominant heating mechanism until extremely large stellar masses.

Now the question is, if one observes a Population III star shining at the Eddington luminosity, what can it tell us about the reaction strength between DM and nucleon? From [9], we already know that $L_{DM} \propto \sigma_n \rho_{DM} M_\star^3 / m_X R_\star^2$. If we keep other parameters like the ambient DM density ρ_{DM} and the stellar mass $M_\star$ and radius $R_\star$ fixed and

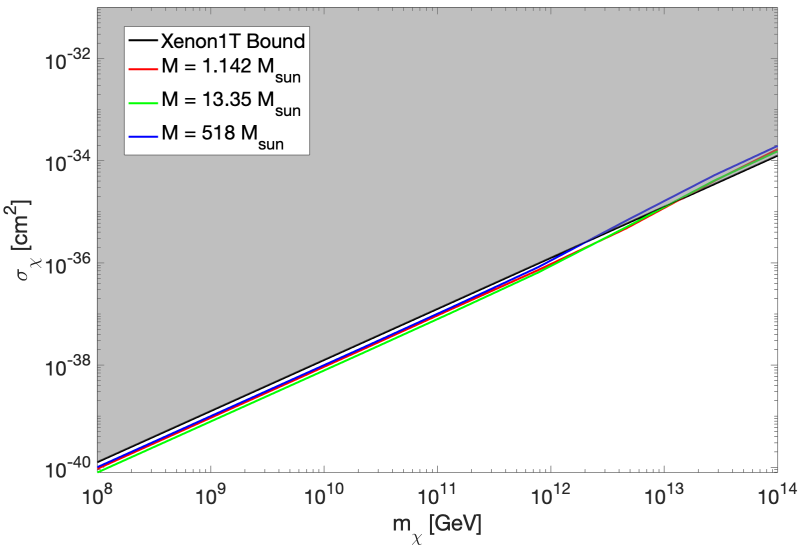

Figure 7: Bounds on dark matter interaction cross section for $M_{max} = 1, 40, 1000 M_\odot$. These were calculated by extracting M_{max} as a function of ρ_χ from the upper mass bounds, and then solving for the cross section which makes the "strong limit" equation (5.2) hold true. The gray region is the exclusion region calculated from the X1T experiment [1].

.

take DM particle mass m_χ as the independent variable, we could then calculate the cross-section constraint σ_n as a function of m_χ. This is equivalent to taking a vertical slice of Figure 6 and finding the cross section corresponding to M_{max} for every ρ_χ. We can do this for a few test cases of $M_{max} = 1, 40, 1000 M_\odot$, and the results of this calculation are presented in Figure 7.

The results in Figure 7 are simply a case study to show that constraining dark matter properties (in this case, simply recovering the X1T bounds on dark matter cross section) are feasible. In practice, future surveys can observe Population III stars shining at the Eddington limit, and with assumptions on dark matter density and maximum mass, can reconstruct the cross section needed for the observations.

6 Discussion and Future Work

The existence of dark matter is still one of the most pressing questions in Cosmology and Particle Physics. Direct detection experiments based on the ground are approaching the sensitivity limits, so new methods of constraining dark matter properties must be explored to make the future search fruitful. There is hope that the next generation of telescopes can supplement the search for dark matter, and this work explored two scenarios in which this might be possible.

Neutron stars can be used right now to constrain dark matter properties by searching in high density environments like the galactic center. We showed that these obser-

vations can place stricter bounds on the dark matter cross section than even the most sensitive ground based experiments while also seeing where these types of searches would be limited. Population III stars are a promising candidate for future observatories to provide complimentary constraints assuming they reach the masses and luminosities other research has derived. In conjunction, these two methods can allow searches for dark matter beyond the neutrino floor and the ability to research dark matter candidates beyond the Standard Model.

Acknowledgments

I would like to thank Cosmin Ilie for the overwhelming support he has given me over all four years at Colgate. From fruitful discussions relating to this research to letting me rant about my classes, he was always there for whatever I needed. Additionally, I would like to thank Saiyang Zhang '19 for lovely discussions of this research and teaching me how to tackle complex problems head-on. I would like to thank Thomas Balonek for the unending support as both my academic advisor and as my friend – always reminding me that I am preparing for the rest of my life in everything I do. I would like to thank Karen Harpp for providing me an outlet from physics and astronomy and for making Colgate a place where I truly learned both in and out of the classroom.

The Physics and Astronomy Class of 2020 class made my work possible from the very first day on campus. I am deeply grateful for the ways in which they have pushed me, and how we all grew together as budding-scientists. Related to this, I express my deepest gratitude to every member of the faculty and staff of Colgate's PHAS department for teaching me not only physics, but how to be a loving, supporting teacher who genuinely cares about their students.

Lastly, I would like to thank my family for all the sacrifices they have made to allow me to succeed. Dennis, Kim, Douglas, Kayley, Sasha, Neil, and Carol – I would not be here without all you have done for me.

References

[1] XENON Collaboration 7 collaboration, *Dark matter search results from a one ton-year exposure of xenon1t*, *Phys. Rev. Lett.* **121** (2018) 111302.

[2] X. Cui, A. Abdukerim, W. Chen, X. Chen, Y. Chen, B. Dong et al., *Dark Matter Results from 54-Ton-Day Exposure of PandaX-II Experiment*, Phys. Rev. Lett. **119** (2017) 181302.

[3] E. Bulbul, M. Markevitch, A. Foster, R. K. Smith, M. Loewenstein and S. W. Randall, *Detection of an unidentified emission line in the stacked x-ray spectrum of galaxy clusters*, *The Astrophysical Journal* **789** (2014) 13.

[4] A. Boyarsky, O. Ruchayskiy, D. Iakubovskyi and J. Franse, *Unidentified line in x-ray spectra of the andromeda galaxy and perseus galaxy cluster*, *Physical Review Letters* **113** (2014) .

[5] G. R. Blumenthal, S. Faber, R. Flores and J. R. Primack, *Contraction of dark matter galactic halos due to baryonic infall*, *The Astrophysical Journal* **301** (1986) 27.

[6] K. Freese, D. Spolyar and A. Aguirre, *Dark matter capture in the first stars: a power source and limit on stellar mass*, *Journal of Cosmology and Astroparticle Physics* **2008** (2008) 014.

[7] A. Gould, *Resonant enhancements in weakly interacting massive particle capture by the earth*, *The Astrophysical Journal* **321** (1987) 571.

[8] I. F. Albuquerque, L. Hui and E. W. Kolb, *High energy neutrinos from superheavy dark matter annihilation*, *Physical Review D* **64** (2001) 083504.

[9] C. Ilie and S. Zhang, *Multiscatter capture of superheavy dark matter by pop III stars*, *JCAP* **2019** (2019) 051 [1908.02700].

[10] J. Bramante, A. Delgado and A. Martin, *Multiscatter stellar capture of dark matter*, Phys. Rev. D **96** (2017) 063002 [1703.04043].

[11] E. Aprile, J. Aalbers, F. Agostini, M. Alfonsi, F. Amaro, M. Anthony et al., *First dark matter search results from the xenon1t experiment*, *Physical review letters* **119** (2017) 181301.

[12] J. Bramante, A. Delgado and A. Martin, *Multiscatter stellar capture of dark matter*, *Physical Review D* **96** (2017) 063002.

[13] G. Bertone and M. Fairbairn, *Compact stars as dark matter probes*, *Phys. Rev. D* **77** (2008) 043515.

[14] C. Kouvaris and P. Tinyakov, *Constraining asymmetric dark matter through observations of compact stars*, Phys. Rev. D **83** (2011) 083512 [1012.2039].

[15] M. McCullough and M. Fairbairn, *Capture of inelastic dark matter in white dwarves*, Phys. Rev. D **81** (2010) 083520 [1001.2737].

[16] XENON Collaboration 4 collaboration, *Constraining the spin-dependent wimp-nucleon cross sections with xenon1t*, *Phys. Rev. Lett.* **122** (2019) 141301.

[17] F. Iocco, *Dark matter capture and annihilation on the first stars: preliminary estimates*, *The Astrophysical Journal Letters* **677** (2008) L1.

[18] R. A. Windhorst, F. Timmes, J. S. B. Wyithe, M. Alpaslan, S. K. Andrews, D. Coe et al., *On the observability of individual population iii stars and their stellar-mass black hole accretion disks through cluster caustic transits*, *The Astrophysical Journal Supplement Series* **234** (2018) 41.

[19] D. Spolyar, K. Freese and P. Gondolo, *Dark matter and the first stars: A new phase of stellar evolution*, *Phys. Rev. Lett.* **100** (2008) 051101.